



RESEARCH LETTER

10.1002/2014GL062053

Key Points:

- Sound velocities of basalt and silicate glasses are measured at high pressure
- Basalt and silicate glasses show acoustic anomalies at high pressures
- Implications for the upper mantle low-velocity zone are discussed

Supporting Information:

- Tables S1–S3 and Figures S1–S4

Correspondence to:

J. Liu,
jinliu@utexas.edu

Citation:

Liu, J., and J.-F. Lin (2014), Abnormal acoustic wave velocities in basaltic and (Fe,Al)-bearing silicate glasses at high pressures, *Geophys. Res. Lett.*, *41*, 8832–8839, doi:10.1002/2014GL062053.

Received 29 SEP 2014

Accepted 4 DEC 2014

Accepted article online 11 DEC 2014

Published online 23 DEC 2014

Abnormal acoustic wave velocities in basaltic and (Fe,Al)-bearing silicate glasses at high pressures

Jin Liu¹ and Jung-Fu Lin¹¹Department of Geological Sciences, Jackson School of Geosciences, University of Texas at Austin, Austin, Texas, USA

Abstract We have measured acoustic V_p and V_s velocities of (Fe,Al)-bearing MgSiO_3 silicate glasses and an Icelandic basalt glass up to 25 GPa. The velocity profiles of the (Fe,Al)-bearing and basaltic silicate glasses display decreased V_p and V_s with minima at approximately 5 and 2 GPa, respectively, which could be explained by the mode softening in the aluminosilicate networks. Our results represent the first observation of such velocity softening extending into the chemically complex basaltic glass at a relatively low transition pressure, which is likely due to its degree of polymerization, while the Fe and Al substitutions reduce sound velocities in MgSiO_3 glass. If the velocity softening in the basaltic and silicate glasses can be used as analogs for understanding melts in Earth's interior, these observations suggest that the melt fraction needed to account for the velocity reduction in the upper mantle low-velocity zone may be smaller than previously thought.

1. Introduction

High-pressure-temperature (P - T) properties of silicate melts in the deep mantle are essential to understanding dynamic processes and chemical evolutions of the planet's interior [Stolper *et al.*, 1981; Mysen *et al.*, 1982; Abe, 1993; Sakamaki *et al.*, 2013; Sanloup *et al.*, 2013]. Of particular interest are properties of the melts and melt-bearing solids including viscosity, density, acoustic wave velocity, and chemical partitioning between melts and surrounding solids. Changes in these properties at high P - T can significantly affect our understanding of the characteristics of plate tectonics motion, the current style of mantle dynamics, as well as the thermal evolution and chemical differentiation of the deep Earth, especially in the early magma ocean [e.g., Mysen, 1983; Ohtani, 1985; Rivers and Carmichael, 1987; Abe, 1993; Webb, 1997; Stixrude and Karki, 2005; Karki and Stixrude, 2010; Murakami and Bass, 2011; Sanloup *et al.*, 2013]. Previous experimental and theoretical studies have shown that silicate melts are typically less dense than the corresponding solids at upper mantle conditions, resulting in a buoyant melt ascending to the Earth's surface as igneous intrusions and plutons. However, at higher pressures relevant to lower mantle conditions, the density contrast between a silicate solid and a relevant silicate melt could be reversed due to the higher compressibility of the melt network as well as the preferential partitioning of heavier incompatible elements (e.g., Fe) into the melts relative to the surrounding solids [Stolper *et al.*, 1981; Stixrude and Karki, 2005; Murakami and Bass, 2011; Nomura *et al.*, 2011; Prescher *et al.*, 2014]. Since studying physical and chemical properties of silicate melts at extreme P - T conditions of the deep mantle remains extremely challenging, silicate glasses have been commonly used as analogs for understanding properties of silicate melts in extreme environments [Williams and Jeanloz, 1988; Lee *et al.*, 2008; Murakami and Bass, 2011].

Previous experimental and theoretical studies have extensively explored structural, thermodynamic, and transport properties of the silicate glasses and melts with various cations and alumina contents including Ca, Mg, and $\text{Fe}^{3+}/\Sigma\text{Fe}$ [e.g., Stolper and Ahrens, 1987; Stixrude and Karki, 2005; Shimoda and Okuno, 2006; Lin *et al.*, 2007; Giordano *et al.*, 2008; Lee *et al.*, 2008; Mosenfelder *et al.*, 2009; Karki and Stixrude, 2010; Sanloup *et al.*, 2013; Wang *et al.*, 2014]. On the other hand, studies on high-pressure elastic properties and acoustic velocities of silicate melts and glasses relevant to the deep-mantle conditions are scarce and have been mostly limited to SiO_2 and MgSiO_3 glasses [e.g., Suito *et al.*, 1992; Zha *et al.*, 1994; Sanchez-Valle and Bass, 2010; Murakami and Bass, 2011; Weigel *et al.*, 2012; Ghosh *et al.*, 2014; Sakamaki *et al.*, 2014]. These studies have shown that silica and silicate glasses exhibit an elastic anomaly and a minimum incompressibility at approximately a few gigapascal (GPa), where the longitudinal and shear acoustic velocities (V_p and V_s) as well as incompressibility decrease with increasing pressure [e.g., Suito *et al.*, 1992; Zha *et al.*, 1994; Sanchez-Valle

and Bass, 2010; Sakamaki et al., 2014]. Such an abnormal elastic behavior has been proposed to be most likely due to significant local structural and topological modifications of the Si-O networks occurring through reductions in the ring sizes and collapses of interstitial void spaces [e.g., Tkachev et al., 2005; Walker et al., 2007; Sanchez-Valle and Bass, 2010; Sato et al., 2011; Shen et al., 2011; Weigel et al., 2012; Sakamaki et al., 2014; Wang et al., 2014]. The observation of the elastic anomaly also raises interests in knowing the sound velocity behavior in chemically complex silicate glasses and melts that are of geochemical relevance, including the basaltic melt composition in the deep crust and mantle conditions. To date, it remains unclear whether or not such sound velocity softening is present in silicate glasses and melts with relevant chemical compositions in natural environments; if such a velocity anomaly persists into the basaltic melt, it would significantly affect our understanding of the properties of melts in the deep Earth.

In this study, we report acoustic wave velocities and derived elastic parameters of four representative silicate glasses at high pressures, including MgSiO₃ glass, Fe-bearing and (Fe,Al)-bearing MgSiO₃ glasses, and an Icelandic basalt glass (BIR-1) using Brillouin light scattering (BLS) spectroscopy in a diamond anvil cell (DAC) up to 25 GPa at room temperature. These results are used to decipher the compositional effects of the Fe, Ca, and Al substitution on acoustic velocities and elastic constants of the MgSiO₃ glass at high pressures. We have observed the acoustic velocity softening in the Icelandic basalt glass at approximately 2 GPa, showing that the softening behavior can also exist in complex, natural silicate glasses. These new results are applied to understand the acoustic wave behaviors of silicate melts and melt-solid mixtures in the low-velocity zone (LVZ) of the upper mantle.

2. Experiments

2.1. Sample Description

Four different silicate glass samples were used as starting materials for the high-pressure Brillouin experiments. Their chemical compositions and homogeneities were examined using electron microprobe and Mössbauer analyses. MgSiO₃, Fe-bearing (Mg_{0.9}Fe_{0.1}SiO₃), and (Fe,Al)-bearing (Mg_{0.79}Fe_{0.10}Al_{0.10}Si_{0.96}O₃) glass samples were synthesized using a high-temperature furnace (see Mao et al. [2014] for more details on the syntheses of the Fe- and (Fe,Al)-bearing glasses). For MgSiO₃ glass, the mechanically mixed and pressed pellet of starting MgO and SiO₂ with 1:1 molar ratio was wrapped in a Pt wire loop and melted in a vertical tube furnace for 1 h. It was then quenched by rapidly removing the sample from the furnace. Electron microprobe and Mössbauer spectroscopy analyses of the 95% ⁵⁷Fe-enriched (Fe,Al)-bearing silicate glass sample show a chemical composition of Mg_{0.79}Fe_{0.10}Al_{0.10}Si_{0.96}O₃ containing 4.97 wt % Al₂O₃ and 7.73 wt % FeO + Fe₂O₃ (78 mol % Fe³⁺ of the total iron) in the sample, while approximately 30% of the total iron contained in the Mg_{0.9}Fe_{0.1}SiO₃ glass is Fe³⁺ (Table S1 in the supporting information). The Icelandic basalt glass (BIR-1) was obtained from the U.S. Geology Survey (USGS), which is one of three USGS mafic rock standard reference glass samples, and has a chemical composition of Na_{0.06}Ca_{0.26}Mg_{0.26}Fe_{0.16}Al_{0.33}Si_{0.88}O₃ with 13.30 wt % CaO, 15.50 wt % Al₂O₃, and 10.40 wt % FeO + Fe₂O₃ (18 mol % Fe³⁺ of all Fe), together with minor amounts of Ti, Mn, and K that are all less than 1 wt % [Gladney and Roelandts, 1988]. The chemical composition of the basaltic glass is similar to abyssal tholeiites, and its density is 2.79 g/cm³ at ambient conditions [Gladney and Roelandts, 1988].

2.2. High-Pressure Brillouin Spectroscopy

Each glass sample with a diameter of approximately 100 μm and a thickness of approximately 40 μm was loaded in a short symmetrical DAC having a pair of 500 μm culets. A rhenium gasket with an initial thickness of 250 μm was preindented to approximately 60 μm thick with a hole of 250 μm in diameter drilled in it to be used as the sample chamber. Ne was used as the pressure medium, while two ruby spheres were also loaded next to the sample and were used as the pressure gauge [Mao et al., 1986]; pressure uncertainties (±1σ) were calculated using multiple measurements of the ruby fluorescence spectra before and after each BLS measurement. High-pressure Brillouin measurements were conducted in the symmetric (platelet) scattering geometry using the JRS Fabry-Perot interferometer equipped with an avalanche photodiode detector (Count-10B Photo Counting Module with approximately 5 c/s from Laser Components, Inc.) and a Coherent Verdi V2 laser with a wavelength of 532 nm having a focused beam size of approximately 20 μm in diameter at the Mineral Physics Laboratory of the University of Texas at Austin [Lu et al., 2013]. The symmetric geometry relates the measured frequency shifts to the acoustic velocities (V_p and V_s) without the need for

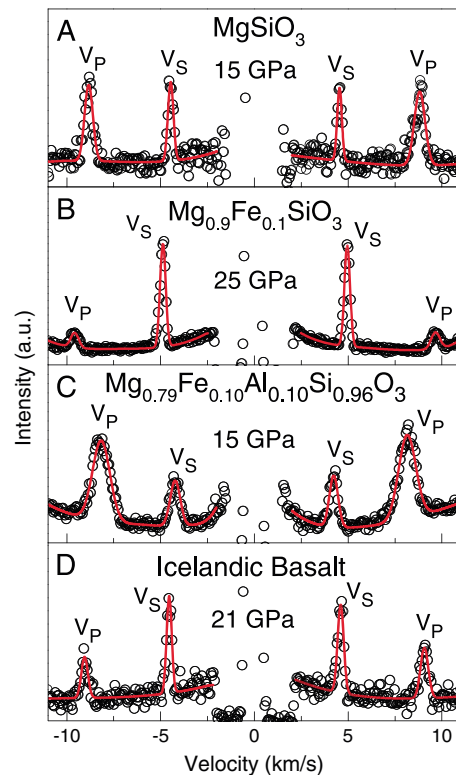


Figure 1. Representative Brillouin spectra of the glasses at high pressure. (a) MgSiO_3 glass at 15 GPa. (b) $\text{Mg}_{0.9}\text{Fe}_{0.1}\text{SiO}_3$ glass at 25 GPa. (c) $\text{Mg}_{0.79}\text{Fe}_{0.10}\text{Al}_{0.10}\text{Si}_{0.96}\text{O}_3$ glass at 15 GPa. (d) Icelandic basalt glass at 21 GPa. Open symbols: experimental data; red solid lines: fitted results.

finite strain equations [Davies and Dziewonski, 1975] (see supporting information for details) (Figures 2–4 and Figures S2–S4 in the supporting information). Since the derivation of the K and G moduli at high pressures typically requires the use of the known density of the glass as an input parameter (which was not measured directly in this study), here we have followed the modeling procedure developed previously in order to derive these parameters [Davies and Dziewonski, 1975; Sanchez-Valle and Bass, 2010; Weigel et al., 2012; Sakamaki et al., 2014]. Briefly, the ν and V_Φ values were directly calculated from the measured acoustic V_P and V_S velocities of each silicate glass sample, whereas the pressure-dependent density was calculated through iterated integration of the V_Φ as a function of pressure using the density at ambient conditions as the initial input parameter. The K and G values can then be determined using measured acoustic velocities and modeled density at corresponding pressures. Finally, these values were used as input parameters for the fitting using the third-order finite strain equations via the least squares regression method in order to derive these elastic parameters (see supporting information for more details). The modeled elastic parameters and density profile of the MgSiO_3 glass are reasonably consistent with the results in a previous study [Sanchez-Valle and Bass, 2010].

The measured V_P and V_S velocities as well as the derived thermoelastic parameters of the glasses up to 25 GPa clearly show two distinct regions with significant changes as a function of pressure (Figure 2). The V_P and V_S velocities of the glasses slightly decrease with increasing pressure up to 2–5 GPa; such velocity softening is much more pronounced in the V_S velocities than the V_P velocities. The V_P and V_S velocities then increase with increasing pressure after the softening transition with the V_P and V_S minima. The derived K , G , and ν of the glasses also exhibit similar abnormal behavior at high pressures. The observation of the velocity softening in the V_P and V_S of the MgSiO_3 glass at approximately 5 GPa is consistent with previous observations [Zha et al., 1994; Tkachev et al., 2005; Sanchez-Valle and Bass, 2010], although first-principle molecular dynamic simulations on the MgSiO_3 glass did not show any visible velocity anomaly at pressures up to

knowing the refractive index [Whitfield et al., 1976]. The scattering angle of the Brillouin system was calibrated using known velocities of distilled water and standard SiO_2 glass at ambient conditions [Mao et al., 2012; Lu et al., 2013]. The precision of the determined velocities of the glass samples at high pressures is typically better than 0.5% in our measurements. Representative Brillouin spectra collected in these glass samples up to approximately 25 GPa and room temperature are displayed in Figure 1 and Figure S1 in the supporting information. The acoustic velocities (V_P and V_S) were determined through Gaussian function fitting to the acoustic peaks using the OriginLab Pro 9.0 program (Table S2 in the supporting information). To examine the possible presence of crystalline phases in our samples at ambient conditions and upon compression, Raman spectra were also recorded from the same samples at every 5 GPa pressure step. These Raman spectra at high pressures exhibit similar spectral features to previous reports for MgSiO_3 glass [Hemley et al., 1986; Kubicki et al., 1992]; no distinct Raman peak for the crystalline phase of SiO_2 and MgSiO_3 was detected within experimental pressures, ruling out the possibility of the presence of crystalline phases in our samples at high pressures.

3. Results and Discussion

The measured acoustic velocities of the glasses were used to derive other thermoelastic parameters including the Poisson's ratio (ν), the bulk sound velocity (V_Φ), density (ρ), and adiabatic bulk modulus (K) and shear modulus (G) and their pressure derivatives (K' and G'), using third-order

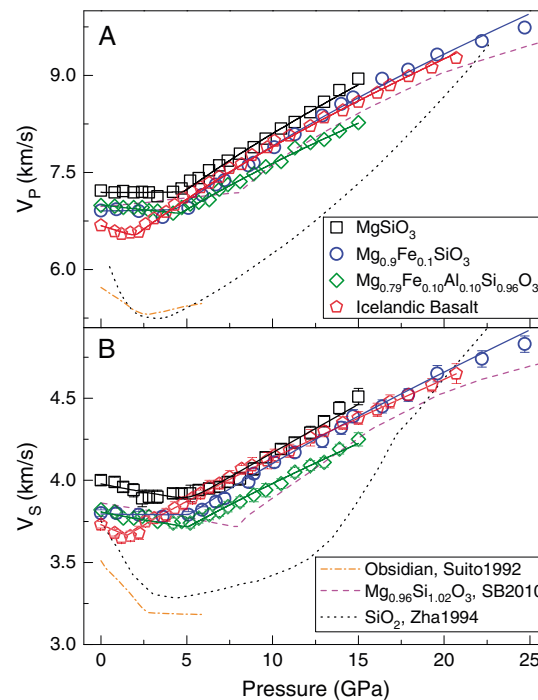


Figure 2. Acoustic wave velocities of the glasses as a function of pressure. (a) Compressional wave velocities (V_p). (b) Shear wave velocities (V_s). Squares: $MgSiO_3$ glass; circles: $Mg_{0.9}Fe_{0.1}SiO_3$ glass; diamonds: $Mg_{0.79}Fe_{0.10}Al_{0.10}Si_{0.96}O_3$ glass; pentagons: Icelandic basalt glass; solid lines: modeled results; dash-dotted lines: obsidian glass (Suito1992) [Suito *et al.*, 1992]; dashed lines: $Mg_{0.96}Fe_{0.12}SiO_3$ glass (SB2010) [Sanchez-Valle and Bass, 2010]; dotted lines: SiO_2 glass (Zha1994) [Zha *et al.*, 1994]; vertical ticks: experimental uncertainties. The errors in velocities and pressures are smaller than the symbols and are not plotted for clarity. We note that the silicate glass sample used by Sanchez-Valle and Bass [2010] contained molar fractions of 0.485 MgO and 0.515 SiO_2 with 6 mol % extra SiO_2 such that the chemical formula derived from the molar fractions of the glass should be $Mg_{0.96}Fe_{0.12}SiO_3$.

The Icelandic basalt glass has the most complex chemistry among all glasses studied here as it contains 47.96 wt % SiO_2 , 9.70 wt % MgO, 10.40 wt % FeO + Fe_2O_3 , 15.50 wt % Al_2O_3 , and 13.30 wt % CaO. Although the basaltic glass displays slower velocities than other silicate glasses at ambient conditions, its velocity profiles are significantly enhanced at high pressures after the softening transition, likely due to the incorporation of the large Ca^{2+} cations that cause a greater disorder in the local structural environment [Stebbins *et al.*, 1997]. We should note that the spin and valence states of Fe^{2+} and Fe^{3+} in the Fe-bearing and (Fe,Al)-bearing glasses remain highly debated and their effects on the elasticity of silicate glasses will need to be further considered in future studies [Nomura *et al.*, 2011; Mao *et al.*, 2014; Prescher *et al.*, 2014]. On the other hand, high-pressure acoustic velocities of garnetite with a chemical composition similar to the mid-ocean ridge basalt (MORB) glass have been reported by Kono *et al.* [2012] using ultrasonic measurements. However, the sintered garnetite sample was produced from a synthetic MORB glass containing majorite and stishovite crystals with grain sizes in the range of 0.5–1.0 μm in diameter. These results showed that the measured V_p is $\sim 13\%$ higher than that of the Icelandic basalt glass studied here. The large velocity difference between these studies of samples having similar chemical compositions may be explained by the presence of crystalline phases in the sample used by Kono *et al.* [2012], because amorphous glasses tend to exhibit relatively lower sound velocities than their crystalline counterparts [Zha *et al.*, 1994; Murakami and Bass, 2011; Ghosh *et al.*, 2014].

170 GPa [Ghosh *et al.*, 2014]. Most importantly, this elastic abnormal behavior is observed to occur not only in Fe-bearing and (Fe,Al)-bearing silicate glasses at approximately 5 GPa but also in the Icelandic basalt glass at approximately 2 GPa, a relatively lower transition pressure as compared to approximately 5 GPa in the $MgSiO_3$ -dominant glasses (Figure 2).

The comparison of the velocity profiles of the silicate and silica glasses before the softening region shows that the end-member $MgSiO_3$ glass generally displays the highest acoustic velocities among all silicate glasses investigated here at high pressures (Figure 2), whereas the silica glass has the lowest-velocity profiles [Zha *et al.*, 1994]. That is, the cation substitution of Fe, Al, and Ca into the $MgSiO_3$ glass reduces the sound velocities at ambient conditions (Figure 2 and Figure S3 in the supporting information). Prior to the completion of the velocity softening in $MgSiO_3$ silicate glasses, the substitution of 10 mol % Fe in $MgSiO_3$ glass decreases the V_p , V_s , and V_ϕ by approximately 3–4%. The comparison of the velocity profiles of the $Mg_{0.9}Fe_{0.1}SiO_3$ and (Fe,Al)-bearing silicate glasses shows that the substitution of 10 mol % alumina into the Fe-bearing glass (10 mol % Fe) slightly increases the sound velocities by less than 1% (the experimental uncertainty in this study is approximately 0.5%). That is, the effect of adding alumina onto Fe-bearing $MgSiO_3$ glass has a relatively small effect on the elasticity of $MgSiO_3$ glass before the velocity anomaly transition. Overall, these observations show that higher SiO_2 content in the glass produces lower acoustic velocities, whereas the higher MgO content enhances the velocity profiles.

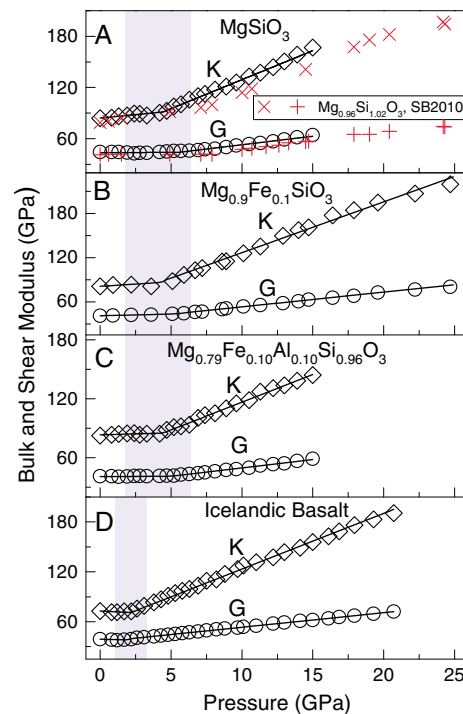


Figure 3. Bulk and shear moduli of the glasses as a function of pressure. (a) MgSiO_3 glass. (b) $\text{Mg}_{0.9}\text{Fe}_{0.1}\text{SiO}_3$ glass. (c) $\text{Mg}_{0.79}\text{Fe}_{0.10}\text{Al}_{0.10}\text{Si}_{0.96}\text{O}_3$ glass. (d) Icelandic basalt glass. Diamonds: experimental bulk modulus (K); circles: experimental shear modulus (G); cross and plus signs: K and G for $\text{Mg}_{0.96}\text{Fe}_{0.12}\text{SiO}_3$ glass (SB2010), respectively [Sanchez-Valle and Bass, 2010]; solid lines: modeled results from the best fit elastic moduli according to the third-order finite strain equation of state [Davies and Dziewonski, 1975]. The shaded areas represent the approximate pressure range of the abnormal velocity behavior and are plotted to guide the eyes. The errors are smaller than the symbols and are not shown for clarity.

transition. Fe substitution moderately decreases both moduli by approximately 5% and has a negligible effect on their pressure derivatives. On the other hand, Al substitution enhances both moduli by 2–3% but slightly reduces the pressure derivatives of the moduli (Table S3 in the supporting information). The calculated density-pressure profiles of all silicate glasses studied here did not show abrupt discontinuities within the pressure range of the velocity softening, consistent with previous studies [Sanchez-Valle and Bass, 2010] (Figure S4 in the supporting information). The Poisson's ratio of the basaltic and silicate glasses displays a jump across the velocity softening. However, the experimentally determined Poisson's ratios of all silicate glass samples are all similar to each other within experimental uncertainties, indicating that there is nearly no appreciable compositional effect on the Poisson's ratio in these silicate glasses (Figure 4). We note that the incompressibility anomaly of silica and MgSiO_3 glasses has been experimentally observed at approximately 5 GPa in previous ultrasonic and Brillouin scattering studies [e.g., Suito *et al.*, 1992; Zha *et al.*, 1994; Sanchez-Valle and Bass, 2010]. Such anomalous velocity softening behavior has been explained as a result of the collapse of interstitial voids as well as the topological rearrangement of the silicate network including the mutual rotation of the local SiO_4 tetrahedra and bending of the Si-O-Si bond [Hemley *et al.*, 1986; Meade and Jeanloz, 1987; Funamori *et al.*, 2004; Sato *et al.*, 2011; Shen *et al.*, 2011; Weigel *et al.*, 2012]. In contrast, theoretical calculations have showed that the acoustic velocities of the MgSiO_3 glass monotonically increase with increasing pressure without any visible anomaly and that the incompressibility is much lower than that

The elasticity of the glasses above the softening regime actually behaves quite differently from that before the transition (Figures 2–4). After the velocity softening, the substitution of 10 mol % Fe in the MgSiO_3 glass reduces the velocity of the MgSiO_3 glass by approximately 2–4%. In contrast, the sound velocities of the (Fe,Al)-bearing silicate glass continuously deviate from that of the MgSiO_3 glass and exhibit lower-velocity profiles by approximately 4–8%. These observations suggest that the additions of both FeO + Fe_2O_3 and Al_2O_3 can reduce the sound velocities of the MgSiO_3 glass and that adding 10 mol % Al into the Fe-bearing glass contributes an additional ~4% reduction in the acoustic velocities of the Fe-bearing silicate glass at a given pressure of 15 GPa. We note that the discrepancy in the pressure-velocity profiles between the MgSiO_3 glass studied here and the vitreous MgSiO_3 -enstatite reported previously [Sanchez-Valle and Bass, 2010] is likely due to the presence of an extra 6 mol % SiO_2 in the vitreous MgSiO_3 -enstatite glass sample. Additionally, SiO_2 glass exhibits higher V_p and V_s values than the silicate glasses at pressures above approximately 20 GPa. Such high-velocity profiles may be interpreted as a result of the electronic bonding transition from the quartz-like (fourfold coordinated) to stishovite-like (sixfold coordinated) local structures in the silica glass [Lin *et al.*, 2007; Lee *et al.*, 2008]. That is, the increase in the coordination number in the silica and silicate glasses can significantly enhance their velocity profiles.

Prior to the completion of the elastic anomaly, the pressure derivatives of the bulk and shear moduli are less than 2 and 0.5, respectively; after the anomaly, their values become much larger, reaching approximately 6 and 2, respectively (Table S3 in the supporting information). That is, the bulk and shear moduli as a function of pressure are very flat with minimal changes before the elastic anomaly but rapidly increase with increasing pressure after the

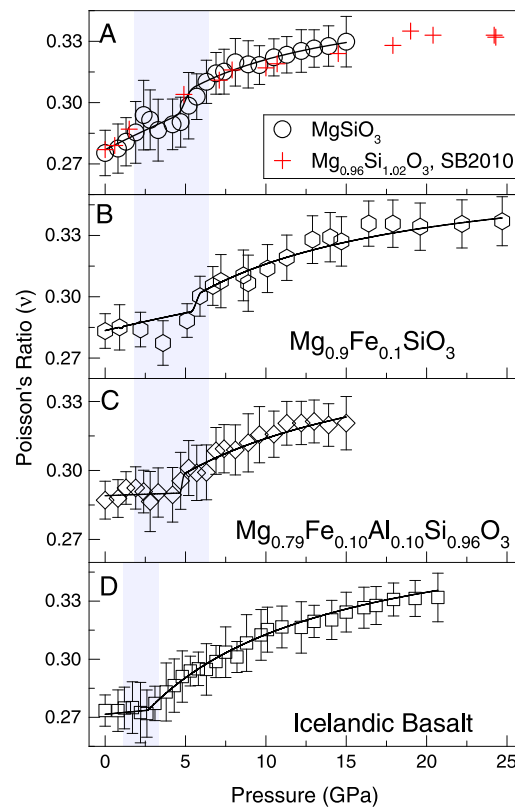


Figure 4. Poisson's ratios (ν) of the glasses as a function of pressure. (a) MgSiO_3 glass. (b) $\text{Mg}_{0.9}\text{Fe}_{0.1}\text{SiO}_3$ glass. (c) $\text{Mg}_{0.79}\text{Fe}_{0.10}\text{Al}_{0.10}\text{Si}_{0.96}\text{O}_3$ glass. (d) Icelandic basalt glass. Open symbols: Poisson's ratios calculated directly from experimental measured velocities; plus signs: Poisson's ratios for MgSiO_3 glass from literature results (SB2010) [Sanchez-Valle and Bass, 2010]; solid lines: modeled results; vertical ticks: representative errors ($\pm 1\sigma$) calculated using standard error propagations.

4. Geophysical Implications

The most compelling observation in our study is that the velocity softening occurs not only in the MgSiO_3 glass but also in chemically complex silicate glasses such as the Icelandic basaltic glass at pressures corresponding to the upper mantle low-velocity zone at a depth of approximately 60–220 km, where low seismic velocities, low viscosity, and high electrical conductivities have been observed [e.g., Hier-Majumder and Courtier, 2011; Sifre et al., 2014]. It should be noted that the velocity anomaly of silicate glasses observed here occurs at the pressure range similar to the viscosity anomaly in basaltic/silicate melts and that both anomalies are likely associated with local structural changes upon compression [Liebske et al., 2005; Sanchez-Valle and Bass, 2010; Sakamaki et al., 2013; Sakamaki et al., 2014; Wang et al., 2014]. Sakamaki et al. [2013] and Wang et al. [2014] have further investigated local structures and viscosity properties of silicate/basaltic melts up to ~ 7 GPa at approximately 1800–2100 K. Specifically, Sakamaki et al. [2013] have found that the changeover in the viscosity behavior for a basaltic magma occurring at approximately 4.5 GPa and 2000 K is accompanied by local structural changes. Suzuki et al. [2005, 2011] have studied the P - T -dependent viscosity of silicate melts in the $\text{CaMgSi}_2\text{O}_6$ - $\text{NaAlSi}_2\text{O}_6$ (diopside-jadeite) system and have found that silicate melt containing 50% diopside-50% jadeite composition displays a changeover in viscosity at 2.5 GPa and 1650 K and at 3.5 GPa and 2073 K. On the other hand, the acoustic velocity of the diopside-jadeite glasses exhibits a minimum at approximately 4–6 GPa and 300 K.

It is thus conceivable that the acoustic softening behavior observed in the silicate/basaltic glasses can also occur in silicate melts at high P - T , which can then affect our understanding of the velocity behavior of silicate

of the experimentally observed values [Shimoda and Okuno, 2006; Ghosh et al., 2014]. These discrepancies between computational and experimental values may be due to the frequency-dependent effect on the elasticity, since the relaxed bulk modulus at low frequency (Hz) in theoretical calculations is expected to be lower than the unrelaxed modulus at high frequency (GHz) in experimental measurements [Rivers and Carmichael, 1987; Meade and Jeanloz, 1987].

The difference in the transition pressures between the basaltic glass and (Fe,Al)-bearing silicate glasses studied here indicates that the substitution of the relatively large Ca^{2+} cation (13.3 wt % CaO in the sample) having sixfold and sevenfold coordinated sites plays a significant role in the high-pressure elastic behavior of the glasses [Cormier and Cuello, 2013]. Ca^{2+} can act as a modifying cation that breaks up the three-dimensional Si-O-Si network, promoting the ion mobility (diffusion) and lowering the melt viscosity [Williams and Jeanloz, 1988]. The low-pressure elastic softening phenomena have been commonly observed in typical oxide glasses containing short-range covalent bonds [Mysen, 1983]. The elastic anomaly at approximately 2 GPa may be associated with the degree of polymerization in silicate glass, which is closely related to composition and the ratio of nonbridging oxygen to tetrahedral cations (T) according to the random network model [Mysen et al., 1982]. Sakamaki et al. [2014] have demonstrated that the sound velocity softening in jadeite, albite, and diopside glasses was caused by the rapid shrinkage of their intermediate-range, locally ordered structures.

melts in the upper mantle low-velocity zone. If the sound velocity softening occurs in the incipient melts present in the upper mantle low-velocity zone, the melt fraction needed to account for the velocity reduction in the region may be less than previously proposed. The relatively low partial melt scenario implied here may help resolve the dilemma between the elevated melt volume fractions and the relative low temperatures (or viscosity/density-driven melt drainage processes) prevailing in the upper asthenosphere [Hermance and Grillo, 1974; McKenzie *et al.*, 2005; Kawakatsu *et al.*, 2009; Hier-Majumder and Courtier, 2011; Sakamaki *et al.*, 2013; Sifre *et al.*, 2014]. Future high *P-T* experimental data on sound velocities of silicate/basaltic melts are urgently needed to better understand the role of silicate melts relevant to the LVZ.

Acknowledgments

We thank J. Kung, H. Watson, and J. Gardner for providing the silicate glass samples. We acknowledge J. Yang, C. McCammon, Y. Wu, and C. Lu for their assistance in the experiments and data analyses. We also thank M. Matheny for editing the manuscript. J.F. Lin acknowledges supports from the U.S. National Science Foundation (EAR-1446946), Energy Frontier Research in Extreme Environments, and Center for High Pressure Science and Advanced Technology (HPSTAR). The Brillouin Light Scattering system was built using financial supports from Carnegie-DOE Alliance Center and Jackson School's Instrumentation Matching Fund. Data used in this study are available from the corresponding author (Jin Liu, e-mail: jinliu@utexas.edu) upon request.

The Editor thanks two anonymous reviewers for their assistance in evaluating this paper.

References

- Abe, Y. (1993), Thermal evolution and chemical differentiation of the terrestrial magma ocean, in *Evolution of the Earth and Planets*, edited by E. Takahashi, R. Jeanloz, and D. Rubie, pp. 41–54, AGU, Washington, D. C.
- Cormier, L., and G. J. Cuello (2013), Structural investigation of glasses along the MgSiO₃-CaSiO₃ join: Diffraction studies, *Geochim. Cosmochim. Acta*, 122, 498–510, doi:10.1016/j.gca.2013.04.026.
- Davies, G. F., and A. M. Dziewonski (1975), Homogeneity and constitution of the Earth's lower mantle and outer core, *Phys. Earth Planet. Inter.*, 10(4), 336–343, doi:10.1016/0031-9201(75)90060-6.
- Funamori, N., S. Yamamoto, T. Yagi, and T. Kikegawa (2004), Exploratory studies of silicate melt structure at high pressures and temperatures by in situ X-ray diffraction, *J. Geophys. Res.*, 109, B03203, doi:10.1029/2003JB002650.
- Ghosh, D. B., B. B. Karki, and L. Stixrude (2014), First-principles molecular dynamics simulations of MgSiO₃ glass: Structure, density, and elasticity at high pressure, *Am. Mineral.*, 99(7), 1304–1314, doi:10.2138/am.2014.4631.
- Giordano, D., J. K. Russell, and D. B. Dingwell (2008), Viscosity of magmatic liquids: A model, *Earth Planet. Sci. Lett.*, 271(1–4), 123–134, doi:10.1016/j.epsl.2008.03.038.
- Gladney, E. S., and I. Roelandts (1988), 1987 compilation of elemental concentration data for USGS BIR-1, DNC-1 and W-2, *Geostandard. Newslett.*, 12(1), 63–118, doi:10.1111/j.1751-908X.1988.tb00044.x.
- Hemley, R. J., H. K. Mao, P. M. Bell, and B. O. Mysen (1986), Raman spectroscopy of SiO₂ glass at high pressure, *Phys. Rev. Lett.*, 57(6), 747–750, doi:10.1103/PhysRevLett.57.747.
- Hermance, J. F., and L. R. Grillo (1974), Constraints on temperatures beneath Iceland from magnetotelluric data, *Phys. Earth Planet. Inter.*, 8(1), 1–12, doi:10.1016/0031-9201(74)90104-6.
- Hier-Majumder, S., and A. Courtier (2011), Seismic signature of small melt fraction atop the transition zone, *Earth Planet. Sci. Lett.*, 308(3–4), 334–342, doi:10.1016/j.epsl.2011.05.055.
- Karki, B. B., and L. P. Stixrude (2010), Viscosity of MgSiO₃ liquid at Earth's mantle conditions: Implications for an early magma ocean, *Science*, 328(5979), 740–742, doi:10.1126/science.1188327.
- Kawakatsu, H., P. Kumar, Y. Takei, M. Shinohara, T. Kanazawa, E. Araki, and K. Suyehiro (2009), Seismic evidence for sharp lithosphere-asthenosphere boundaries of oceanic plates, *Science*, 324(5926), 499–502.
- Kono, Y., T. Irifune, H. Ohfuji, Y. Higo, and K.-I. Funakoshi (2012), Sound velocities of MORB and absence of a basaltic layer in the mantle transition region, *Geophys. Res. Lett.*, 39, L24306, doi:10.1029/2012GL054009.
- Kubicki, J. D., R. J. Hemley, and A. M. Hofmeister (1992), Raman and infrared study of pressure-induced structural changes in MgSiO₃, CaMgSi₂O₆, and CaSiO₃ glasses, *Am. Mineral.*, 77(3–4), 258–269.
- Lee, S. K., *et al.* (2008), X-ray Raman scattering study of MgSiO₃ glass at high pressure: Implication for triclustered MgSiO₃ melt in Earth's mantle, *Proc. Natl. Acad. Sci. U.S.A.*, 105(23), 7925–7929, doi:10.1073/pnas.0802667105.
- Lieske, C., B. Schmickler, H. Terasaki, B. T. Poe, A. Suzuki, K.-I. Funakoshi, R. Ando, and D. C. Rubie (2005), Viscosity of peridotite liquid up to 13 GPa: Implications for magma ocean viscosities, *Earth Planet. Sci. Lett.*, 240, 589–604, doi:10.1016/j.epsl.2005.10.004.
- Lin, J.-F., *et al.* (2007), Electronic bonding transition in compressed SiO₂ glass, *Phys. Rev. B*, 75(1), 012201, doi:10.1103/PhysRevB.75.012201.
- Lu, C., Z. Mao, J.-F. Lin, K. K. Zhuravlev, S. N. Tkachev, and V. B. Prakapenka (2013), Elasticity of single-crystal iron-bearing pyrope up to 20 GPa and 750 K, *Earth Planet. Sci. Lett.*, 361, 134–142, doi:10.1016/j.epsl.2012.11.041.
- Mao, H.-K., J. Xu, and P. M. Bell (1986), Calibration of the ruby pressure gauge to 800 kbar under quasi-hydrostatic conditions, *J. Geophys. Res.*, 91(B5), 4673–4676, doi:10.1029/JB091iB05p04673.
- Mao, Z., J.-F. Lin, S. D. Jacobsen, T. S. Duffy, Y.-Y. Chang, J. R. Smyth, D. J. Frost, E. H. Hauri, and V. B. Prakapenka (2012), Sound velocities of hydrous ringwoodite to 16 GPa and 673 K, *Earth Planet. Sci. Lett.*, 331–332, 112–119, doi:10.1016/j.epsl.2012.03.001.
- Mao, Z., J.-F. Lin, J. Yang, J. Wu, H. C. Watson, Y. Xiao, P. Chow, and J. Zhao (2014), Spin and valence states of iron in Al-bearing silicate glass at high pressures studied by synchrotron Mössbauer and X-ray emission spectroscopy, *Am. Mineral.*, 99(2–3), 415–423, doi:10.2138/am.2014.4490.
- McKenzie, D., J. Jackson, and K. Priestley (2005), Thermal structure of oceanic and continental lithosphere, *Earth Planet. Sci. Lett.*, 233(3–4), 337–349, doi:10.1016/j.epsl.2005.02.005.
- Meade, C., and R. Jeanloz (1987), Frequency-dependent equation of state of fused silica to 10 GPa, *Phys. Rev. B*, 35(1), 236–244.
- Mosenfelder, J. L., P. D. Asimow, D. J. Frost, D. C. Rubie, and T. J. Ahrens (2009), The MgSiO₃ system at high pressure: Thermodynamic properties of perovskite, postperovskite, and melt from global inversion of shock and static compression data, *J. Geophys. Res.*, 114, B01203, doi:10.1029/2008JB005900.
- Murakami, M., and J. D. Bass (2011), Evidence of denser MgSiO₃ glass above 133 gigapascal (GPa) and implications for remnants of ultradense silicate melt from a deep magma ocean, *Proc. Natl. Acad. Sci. U.S.A.*, 108(42), 17,286–17,289, doi:10.1073/pnas.1109748108.
- Mysen, B. O. (1983), The structure of silicate melts, *Annu. Rev. Earth Planet. Sci.*, 11(1), 75–97, doi:10.1146/annurev.ea.11.050183.000451.
- Mysen, B. O., D. Virgo, and F. A. Seifert (1982), The structure of silicate melts: Implications for chemical and physical properties of natural magma, *Rev. Geophys.*, 20(3), 353–383, doi:10.1029/RG020i003p00353.
- Nomura, R., H. Ozawa, S. Tateno, K. Hirose, J. Hernlund, S. Muto, H. Ishii, and N. Hiraoka (2011), Spin crossover and iron-rich silicate melt in the Earth's deep mantle, *Nature*, 473(7346), 199–202, doi:10.1038/nature09940.
- Ohtani, E. (1985), The primordial terrestrial magma ocean and its implication for stratification of the mantle, *Phys. Earth Planet. Inter.*, 38(1), 70–80, doi:10.1016/0031-9201(85)90123-2.

- Prescher, C., C. Weigel, C. McCammon, O. Narygina, V. Potapkin, I. Kuppenko, R. Sinmyo, A. I. Chumakov, and L. Dubrovinsky (2014), Iron spin state in silicate glass at high pressure: Implications for melts in the Earth's lower mantle, *Earth Planet. Sci. Lett.*, *385*, 130–136, doi:10.1016/j.epsl.2013.10.040.
- Rivers, M. L., and I. S. E. Carmichael (1987), Ultrasonic studies of silicate melts, *J. Geophys. Res.*, *92*(B9), 9247–9270, doi:10.1029/JB092iB09p09247.
- Sakamaki, T., A. Suzuki, E. Ohtani, H. Terasaki, S. Urakawa, Y. Katayama, K.-I. Funakoshi, Y. Wang, J. W. Hernlund, and M. D. Ballmer (2013), Ponded melt at the boundary between the lithosphere and asthenosphere, *Nat. Geosci.*, *6*(12), 1041–1044, doi:10.1038/ngeo1982.
- Sakamaki, T., Y. Kono, Y. Wang, C. Park, T. Yu, Z. Jing, and G. Shen (2014), Contrasting sound velocity and intermediate-range structural order between polymerized and depolymerized silicate glasses under pressure, *Earth Planet. Sci. Lett.*, *391*, 288–295, doi:10.1016/j.epsl.2014.02.008.
- Sanchez-Valle, C., and J. D. Bass (2010), Elasticity and pressure-induced structural changes in vitreous MgSiO₃-enstatite to lower mantle pressures, *Earth Planet. Sci. Lett.*, *295*(3–4), 523–530, doi:10.1016/j.epsl.2010.04.034.
- Sanloup, C., J. W. E. Drewitt, Z. Konopkova, P. Dalladay-Simpson, D. M. Morton, N. Rai, W. van Westrenen, and W. Morgenroth (2013), Structural change in molten basalt at deep mantle conditions, *Nature*, *503*(7474), 104–107, doi:10.1038/nature12668.
- Sato, T., N. Funamori, and T. Yagi (2011), Helium penetrates into silica glass and reduces its compressibility, *Nat. Commun.*, *2*(345), 1–5, doi:10.1038/ncomms1343.
- Shen, G., Q. Mei, V. B. Prakapenka, P. Lazor, S. Sinogeikin, Y. Meng, and C. Park (2011), Effect of helium on structure and compression behavior of SiO₂ glass, *Proc. Natl. Acad. Sci. U.S.A.*, *108*(15), 6004–6007, doi:10.1073/pnas.1102361108.
- Shimoda, K., and M. Okuno (2006), Molecular dynamics study of CaSiO₃-MgSiO₃ glasses under high pressure, *J. Phys. Condens. Matter*, *18*(28), 6531, doi:10.1088/0953-8984/18/28/008.
- Sifre, D., E. Gardes, M. Massuyeau, L. Hashim, S. Hier-Majumder, and F. Gaillard (2014), Electrical conductivity during incipient melting in the oceanic low-velocity zone, *Nature*, *509*(7498), 81–85, doi:10.1038/nature13245.
- Stebbins, J. F., J. V. Oglesby, and Z. Xu (1997), Disorder among network-modifier cations in silicate glasses: New constraints from triple-quantum ¹⁷O NMR, *Am. Mineral.*, *82*(11–12), 1116–1124.
- Stixrude, L., and B. Karki (2005), Structure and freezing of MgSiO₃ liquid in Earth's lower mantle, *Science*, *310*(5746), 297–299, doi:10.1126/science.1116952.
- Stolper, E. M., and T. J. Ahrens (1987), On the nature of pressure-induced coordination changes in silicate melts and glasses, *Geophys. Res. Lett.*, *14*(12), 1231–1233, doi:10.1029/GL014i012p01231.
- Stolper, E., D. Walker, B. H. Hager, and J. F. Hays (1981), Melt segregation from partially molten source regions: The importance of melt density and source region size, *J. Geophys. Res.*, *86*(B7), 6261–6271, doi:10.1029/JB086iB07p06261.
- Suito, K., M. Miyoshi, T. Sasakura, and H. Fujisawa (1992), Elastic properties of obsidian, vitreous SiO₂, and vitreous GeO₂ under high pressure up to 6 GPa, in *High-Pressure Research: Application to Earth and Planetary Sciences*, edited by Y. S. A. H. Manghnani, pp. 219–225, AGU, Washington, D. C.
- Suzuki, A., E. Ohtani, H. Terasaki, and K.-I. Funakoshi (2005), Viscosity of silicate melts in CaMgSi₂O₆-NaAlSi₂O₆ system at high pressure, *Phys. Chem. Miner.*, *32*(2), 140–145, doi:10.1007/s00269-005-0452-0.
- Suzuki, A., E. Ohtani, H. Terasaki, K. Nishida, H. Hayashi, T. Sakamaki, Y. Shibazaki, and T. Kikegawa (2011), Pressure and temperature dependence of the viscosity of a NaAlSi₂O₆ melt, *Phys. Chem. Miner.*, *38*(1), 59–64, doi:10.1007/s00269-010-0381-4.
- Tkachev, S. N., M. H. Manghnani, and Q. Williams (2005), In situ Brillouin spectroscopy of a pressure-induced apparent second-order transition in a silicate glass, *Phys. Rev. Lett.*, *95*(5), 057402, doi:10.1103/PhysRevLett.95.057402.
- Walker, A. M., L. A. Sullivan, K. Trachenko, R. P. Bruin, T. O. H. White, M. T. Dove, R. P. Tyer, I. T. Todorov, and S. A. Wells (2007), The origin of the compressibility anomaly in amorphous silica: A molecular dynamics study, *J. Phys. Condens. Matter*, *19*(27), 275,210.
- Wang, Y., T. Sakamaki, L. B. Skinner, Z. Jing, T. Yu, Y. Kono, C. Park, G. Shen, M. L. Rivers, and S. R. Sutton (2014), Atomistic insight into viscosity and density of silicate melts under pressure, *Nat. Commun.*, *5*, 3241, doi:10.1038/ncomms4241.
- Webb, S. (1997), Silicate melts: Relaxation, rheology, and the glass transition, *Rev. Geophys.*, *35*(2), 191–218, doi:10.1029/96RG03263.
- Weigel, C., A. Polian, M. Kint, B. Rufflé, M. Foret, and R. Vacher (2012), Vitreous silica distends in helium gas: Acoustic versus static compressibilities, *Phys. Rev. Lett.*, *109*(24), 245,504, doi:10.1103/PhysRevLett.109.245504.
- Whitfield, C. H., E. M. Brody, and W. A. Bassett (1976), Elastic moduli of NaCl by Brillouin scattering at high pressure in a diamond anvil cell, *Rev. Sci. Instrum.*, *47*(8), 942–947, doi:10.1063/1.1134778.
- Williams, Q., and R. Jeanloz (1988), Spectroscopic evidence for pressure-induced coordination changes in silicate glasses and melts, *Science*, *239*(4842), 902–905, doi:10.1126/science.239.4842.902.
- Zha, C.-S., R. J. Hemley, H.-K. Mao, T. S. Duffy, and C. Meade (1994), Acoustic velocities and refractive index of SiO₂ glass to 57.5 GPa by Brillouin scattering, *Phys. Rev. B*, *50*(18), 13,105–13,112, doi:10.1103/PhysRevB.50.13105.

1 Auxiliary Material for

2 **Abnormal Acoustic Wave Velocities of Basaltic and (Fe,Al)-Bearing Silicate Glasses at**

3 **High Pressures**

4 Jin Liu¹, Jung-Fu Lin¹

5 ¹ Department of Geological Sciences, Jackson School of Geosciences, The University of Texas at
6 Austin, Austin, Texas, USA

7 Corresponding author: Jin Liu (jinliu@utexas.edu)

8 Geophysical Research Letters, 2014

9
10 **Introduction**

11 Here we provide additional information for experimental and modeling results.

12 1. The file of Auxilliary_Material.doc includes related mathematical formulas, two supplemental
13 tables, and four supplemental figures:

14 1.1 Table S1. Chemical compositions of the basaltic glass and synthetic silicate glasses.

15 1.2 Table S2. Acoustic velocities and density of the glasses at high pressure.

16 1.3 Table S3. Bulk and shear modulus of the glasses at ambient conditions and the pressure
17 derivatives of the moduli.

18 1.4 Figure S1. Representative Brillouin spectra of the glasses at ambient conditions.

19 1.5 Figure S2. Bulk sound velocities of the glasses as a function of pressure.

20 1.6 Figure S3. Velocity differences using MgSiO₃ glass as the standard at high pressure.

21 1.7 Figure S4. Density and relative change in density of the glasses at high pressure.

22 **Mathematical formulas**

23 The bulk sound velocity (V_ϕ) and Poisson's ratio (ν) are directly calculated from measured acoustic
24 velocities using the following equations:

25
$$V_\phi^2 = V_P^2 - \frac{4}{3}V_S^2,$$

26 and
$$\nu = \frac{1}{2} \frac{(V_P/V_S)^2 - 2}{(V_P/V_S)^2 - 1},$$

27 where V_P and V_S are compressional and shear wave velocities, respectively. The density (ρ) of the
28 glasses under high pressure is calculated using the following equation:

29
$$\rho = \rho_0 + \int_{P_0}^P 1 / (V_P^2 - \frac{4}{3}V_S^2) dP,$$

30 where ρ_0 is the density at ambient conditions and P_0 is the pressure at ambient conditions [*Sanchez-*
31 *Valle and Bass*, 2010]. Details of the integration method used here have been reported and
32 discussed previously [*Sanchez-Valle and Bass*, 2010]. With the calculated density, the
33 experimental bulk (K) and shear (G) modulus are derived from the following equations:

34
$$K = \rho(V_P^2 - \frac{4}{3}V_S^2),$$

35 and
$$G = \rho V_S^2.$$

36

37 Following the modeling procedure reported by *Sanchez-Valle and Bass* [2010], we have also
38 used the third-order finite strain equations to model the compressional acoustic and equation of
39 state behavior of the glasses at high pressures [*Davies and Dziewonski*, 1975]. The finite-strain
40 equations used here are expressed in the following equations [*Davies and Dziewonski*, 1975]:

41
$$\rho V_P^2 = (1 - 2\varepsilon)^{5/2} (L_1 + L_2 \varepsilon),$$

42 $\rho V_s^2 = (1 - 2\varepsilon)^{5/2} (M_1 + M_2 \varepsilon),$

43 $P = -(1 - 2\varepsilon)^{5/2} (C_1 \varepsilon + C_2 \varepsilon^2 / 2),$

44 where the strain ε is given by:

45 $\varepsilon = \frac{1}{2} [1 - (\frac{\rho}{\rho_0})^{2/3}],$

46 and the coefficients are defined as:

47 $L_1 = K_0 + 4G_0 / 3,$

48 $L_2 = 5L_1 - K_0(3K' + 4G'),$

49 $M_1 = G_0$

50 $M_2 = 5G_0 - 3K_0 G'$

51 $C_1 = 3L_1 - 4M_1,$

52 $C_2 = 3L_2 - 4M_2 + 7C_1,$

53 where K_0 , G_0 , K' and G' are the adiabatic bulk modulus and shear modulus at ambient pressure
54 and their pressure derivatives, respectively. We note that the slight mismatch between our fitting
55 and the high-pressure data is attributed to the inadequacy of the third-order finite strain equations
56 in describing the anomalous velocities of the glasses in Figure 2. Future results on the density of
57 the glasses as function of pressure will help improve the misfits here and add to a better
58 understanding of the acoustic behavior of the glasses at high pressures.

59 **References**

60 Davies, G. F., and A. M. Dziewonski (1975), Homogeneity and constitution of the Earth's lower
61 mantle and outer core, *Phys. Earth Planet. Inter.*, 10(4), 336-343, doi:10.1016/0031-
62 9201(75)90060-6.

63 Sanchez-Valle, C., and J. D. Bass (2010), Elasticity and pressure-induced structural changes in
64 vitreous MgSiO₃-enstatite to lower mantle pressures, *Earth Planet. Sci. Lett.*, 295(3–4), 523-530,
65 doi:10.1016/j.epsl.2010.04.034.

66 Gladney, E. S., and I. Roelandts (1988), 1987 compilation of elemental concentration data for
67 USGS BIR-1, DNC-1 and W-2, *Geostandard. Newslett.*, 12(1), 63-118, doi:10.1111/j.1751-
68 908X.1988.tb00044.x.

69 **Table S1.** Chemical compositions of the Icelandic basaltic glass and synthetic silicate glasses.
 70 The compositions listed are based on electron microprobe analyses, with the unit of wt% in the
 71 table.

	Icelandic Basalt Glass*	MgSiO ₃ Glass	Mg _{0.9} Fe _{0.1} SiO ₃ Glass	Mg _{0.79} Fe _{0.10} Al _{0.10} Si _{0.96} O ₃ Glass
SiO ₂	47.96	59.89	57.82	56.25
Al ₂ O ₃	15.50	-	-	4.97
CaO	13.30	-	-	-
MgO	9.70	40.11	34.92	31.05
FeO	8.34	-	4.90	1.57
Fe ₂ O ₃	2.06	-	2.33	6.16
Na ₂ O	1.82	-	-	-
TiO ₂	0.96	-	-	-
MnO	0.18	-	-	-
K ₂ O	0.03	-	-	-

72 *Obtained from *Gladney and Roelandts* [1988].

73 **Table S2.** Acoustic Velocities and Density of the Glass Samples at High Pressure

Pressure (GPa)	V_P (km/s)	V_S (km/s)	Density (g/cm ³)
<i>MgSiO₃ Glass</i>			
ambient	7.22 (±0.03)	4.00 (±0.03)	2.75 (±0.01)
0.8 (±0.1)	7.19 (±0.04)	3.99 (±0.03)	2.78 (±0.01)
1.3 (±0.1)	7.21 (±0.04)	3.96 (±0.03)	2.79 (±0.01)
1.9 (±0.1)	7.19 (±0.05)	3.94 (±0.04)	2.81 (±0.01)
2.4 (±0.1)	7.20 (±0.05)	3.89 (±0.05)	2.83 (±0.01)
2.8 (±0.2)	7.19 (±0.05)	3.90 (±0.04)	2.84 (±0.01)
3.3 (±0.1)	7.13 (±0.05)	3.90 (±0.04)	2.86 (±0.01)
4.2 (±0.1)	7.20 (±0.05)	3.92 (±0.03)	2.89 (±0.01)
4.7 (±0.1)	7.25 (±0.05)	3.92 (±0.03)	2.90 (±0.01)
5.2 (±0.2)	7.37 (±0.05)	3.92 (±0.05)	2.92 (±0.01)
5.7 (±0.2)	7.41 (±0.05)	3.94 (±0.03)	2.93 (±0.01)
6.3 (±0.2)	7.53 (±0.05)	3.95 (±0.03)	2.95 (±0.01)
6.9 (±0.2)	7.61 (±0.05)	3.96 (±0.03)	2.97 (±0.01)
7.4 (±0.3)	7.68 (±0.06)	3.99 (±0.03)	2.98 (±0.01)
8.1 (±0.2)	7.79 (±0.05)	4.01 (±0.04)	3.00 (±0.01)
8.9 (±0.3)	7.89 (±0.05)	4.07 (±0.04)	3.02 (±0.01)
9.6 (±0.2)	8.02 (±0.05)	4.14 (±0.03)	3.03 (±0.01)
10.5 (±0.3)	8.18 (±0.05)	4.19 (±0.03)	3.06 (±0.01)
11.3 (±0.3)	8.28 (±0.05)	4.23 (±0.03)	3.07 (±0.01)
12.2 (±0.3)	8.43 (±0.05)	4.29 (±0.04)	3.09 (±0.01)
13.0 (±0.3)	8.59 (±0.06)	4.36 (±0.03)	3.11 (±0.01)
13.9 (±0.3)	8.77 (±0.05)	4.44 (±0.04)	3.13 (±0.01)
15.0 (±0.3)	8.95 (±0.07)	4.51 (±0.05)	3.15 (±0.01)
<i>Mg_{0.9}Fe_{0.1}SiO₃ Glass</i>			
ambient	6.91 (±0.03)	3.80 (±0.02)	2.84 (±0.01)
0.9 (±0.1)	6.93 (±0.03)	3.80 (±0.03)	2.87 (±0.01)
2.2 (±0.1)	6.90 (±0.03)	3.79 (±0.02)	2.92 (±0.01)
3.6 (±0.1)	6.81 (±0.02)	3.78 (±0.03)	2.97 (±0.01)
5.1 (±0.1)	6.95 (±0.03)	3.79 (±0.02)	3.02 (±0.01)
5.9 (±0.1)	7.15 (±0.05)	3.82 (±0.02)	3.04 (±0.01)
6.7 (±0.1)	7.31 (±0.03)	3.87 (±0.03)	3.07 (±0.01)
7.2 (±0.1)	7.38 (±0.07)	3.89 (±0.03)	3.08 (±0.01)
8.6 (±0.2)	7.61 (±0.07)	3.99 (±0.03)	3.12 (±0.01)
8.9 (±0.2)	7.65 (±0.08)	4.04 (±0.03)	3.13 (±0.01)
10.1 (±0.2)	7.89 (±0.07)	4.11 (±0.03)	3.16 (±0.01)
11.3 (±0.2)	8.09 (±0.07)	4.17 (±0.03)	3.19 (±0.01)
12.9 (±0.2)	8.38 (±0.07)	4.24 (±0.04)	3.23 (±0.01)
14.0 (±0.2)	8.56 (±0.08)	4.32 (±0.04)	3.25 (±0.01)
14.7 (±0.2)	8.66 (±0.08)	4.39 (±0.04)	3.27 (±0.01)

16.4 (± 0.2)	8.95 (± 0.08)	4.45 (± 0.04)	3.30 (± 0.01)
17.9 (± 0.2)	9.09 (± 0.09)	4.52 (± 0.04)	3.33 (± 0.01)
19.6 (± 0.2)	9.32 (± 0.07)	4.65 (± 0.05)	3.36 (± 0.01)
22.2 (± 0.3)	9.53 (± 0.08)	4.74 (± 0.05)	3.40 (± 0.01)
24.7 (± 0.4)	9.74 (± 0.09)	4.83 (± 0.05)	3.44 (± 0.01)

Mg_{0.79}Fe_{0.10}Al_{0.10}Si_{0.96}O₃ Glass

ambient	6.99 (± 0.03)	3.82 (± 0.02)	2.81 (± 0.01)
0.8 (± 0.1)	6.98 (± 0.03)	3.81 (± 0.02)	2.84 (± 0.01)
1.3 (± 0.1)	6.96 (± 0.02)	3.77 (± 0.02)	2.85 (± 0.01)
1.9 (± 0.1)	6.96 (± 0.04)	3.77 (± 0.02)	2.87 (± 0.01)
2.4 (± 0.1)	6.96 (± 0.04)	3.78 (± 0.02)	2.89 (± 0.01)
2.8 (± 0.2)	6.91 (± 0.05)	3.78 (± 0.03)	2.91 (± 0.01)
3.3 (± 0.1)	6.90 (± 0.05)	3.75 (± 0.02)	2.92 (± 0.01)
4.2 (± 0.1)	6.87 (± 0.04)	3.74 (± 0.03)	2.95 (± 0.01)
4.7 (± 0.1)	6.96 (± 0.05)	3.75 (± 0.03)	2.97 (± 0.01)
5.2 (± 0.2)	7.01 (± 0.05)	3.74 (± 0.03)	2.99 (± 0.01)
5.7 (± 0.2)	7.04 (± 0.05)	3.77 (± 0.03)	3.00 (± 0.01)
6.3 (± 0.2)	7.08 (± 0.05)	3.79 (± 0.03)	3.02 (± 0.01)
6.9 (± 0.2)	7.24 (± 0.04)	3.81 (± 0.03)	3.04 (± 0.01)
7.4 (± 0.3)	7.31 (± 0.04)	3.84 (± 0.03)	3.06 (± 0.01)
8.1 (± 0.2)	7.36 (± 0.05)	3.87 (± 0.03)	3.08 (± 0.01)
8.9 (± 0.3)	7.48 (± 0.05)	3.91 (± 0.04)	3.10 (± 0.01)
9.6 (± 0.2)	7.59 (± 0.05)	3.94 (± 0.04)	3.12 (± 0.01)
10.5 (± 0.3)	7.67 (± 0.05)	3.98 (± 0.03)	3.14 (± 0.01)
11.3 (± 0.3)	7.88 (± 0.05)	4.05 (± 0.03)	3.16 (± 0.01)
12.2 (± 0.3)	7.96 (± 0.05)	4.09 (± 0.03)	3.19 (± 0.01)
13.0 (± 0.3)	8.01 (± 0.05)	4.11 (± 0.03)	3.21 (± 0.01)
13.9 (± 0.3)	8.14 (± 0.05)	4.19 (± 0.03)	3.23 (± 0.01)
15.0 (± 0.3)	8.27 (± 0.06)	4.25 (± 0.04)	3.25 (± 0.01)

Icelandic Basalt Glass

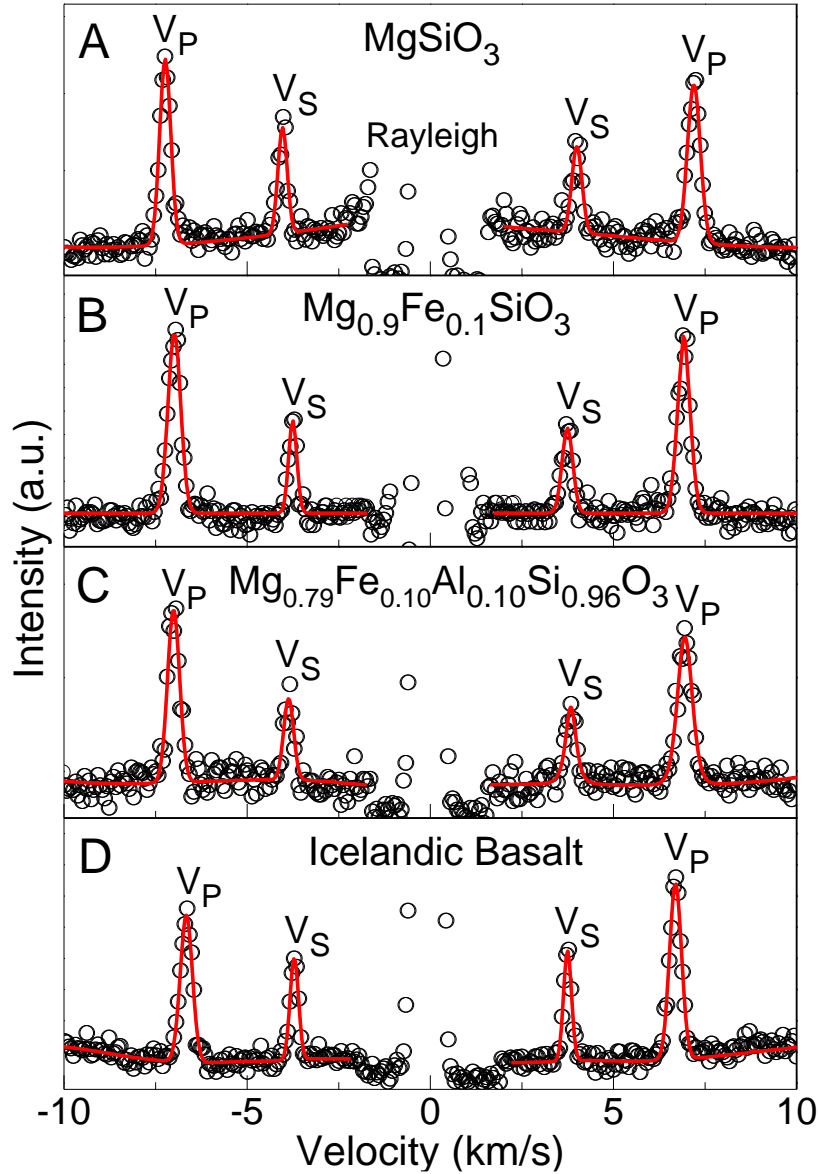
ambient	6.68 (± 0.02)	3.73 (± 0.02)	2.79 (± 0.01)
0.8 (± 0.1)	6.59 (± 0.04)	3.68 (± 0.02)	2.82 (± 0.01)
1.2 (± 0.1)	6.55 (± 0.03)	3.65 (± 0.03)	2.84 (± 0.01)
1.7 (± 0.1)	6.57 (± 0.04)	3.66 (± 0.03)	2.86 (± 0.01)
2.2 (± 0.1)	6.58 (± 0.03)	3.68 (± 0.04)	2.88 (± 0.01)
2.6 (± 0.1)	6.70 (± 0.03)	3.75 (± 0.03)	2.89 (± 0.01)
3.1 (± 0.1)	6.79 (± 0.03)	3.77 (± 0.02)	2.91 (± 0.01)
3.8 (± 0.1)	6.89 (± 0.04)	3.79 (± 0.04)	2.94 (± 0.01)
4.3 (± 0.1)	7.00 (± 0.03)	3.83 (± 0.04)	2.95 (± 0.01)
4.8 (± 0.1)	7.11 (± 0.03)	3.86 (± 0.04)	2.97 (± 0.01)
5.3 (± 0.1)	7.20 (± 0.03)	3.89 (± 0.02)	2.99 (± 0.01)
5.8 (± 0.1)	7.27 (± 0.04)	3.92 (± 0.02)	3.00 (± 0.01)

6.3 (± 0.2)	7.34 (± 0.04)	3.96 (± 0.04)	3.02 (± 0.01)
6.9 (± 0.2)	7.43 (± 0.04)	3.98 (± 0.02)	3.03 (± 0.01)
7.5 (± 0.2)	7.57 (± 0.05)	4.02 (± 0.04)	3.05 (± 0.01)
8.2 (± 0.2)	7.63 (± 0.04)	4.07 (± 0.02)	3.07 (± 0.01)
8.8 (± 0.2)	7.77 (± 0.05)	4.09 (± 0.05)	3.09 (± 0.01)
9.7 (± 0.2)	7.89 (± 0.03)	4.12 (± 0.05)	3.11 (± 0.01)
10.1 (± 0.2)	7.99 (± 0.05)	4.15 (± 0.04)	3.12 (± 0.01)
11.0 (± 0.2)	8.07 (± 0.04)	4.18 (± 0.04)	3.14 (± 0.01)
12.2 (± 0.2)	8.22 (± 0.05)	4.26 (± 0.05)	3.17 (± 0.01)
13.0 (± 0.2)	8.35 (± 0.04)	4.30 (± 0.03)	3.19 (± 0.01)
14.1 (± 0.3)	8.46 (± 0.04)	4.35 (± 0.04)	3.21 (± 0.01)
15.0 (± 0.3)	8.59 (± 0.05)	4.38 (± 0.04)	3.23 (± 0.01)
16.1 (± 0.3)	8.73 (± 0.06)	4.43 (± 0.04)	3.25 (± 0.01)
16.9 (± 0.3)	8.85 (± 0.05)	4.48 (± 0.04)	3.27 (± 0.01)
17.9 (± 0.3)	8.99 (± 0.06)	4.52 (± 0.03)	3.29 (± 0.01)
19.3 (± 0.3)	9.12 (± 0.05)	4.58 (± 0.04)	3.31 (± 0.01)
20.7 (± 0.3)	9.27 (± 0.05)	4.65 (± 0.06)	3.34 (± 0.01)

75 **Table S3.** Modeled Bulk and Shear Moduli of the Glasses at Ambient Conditions and Their
 76 pressure derivatives.

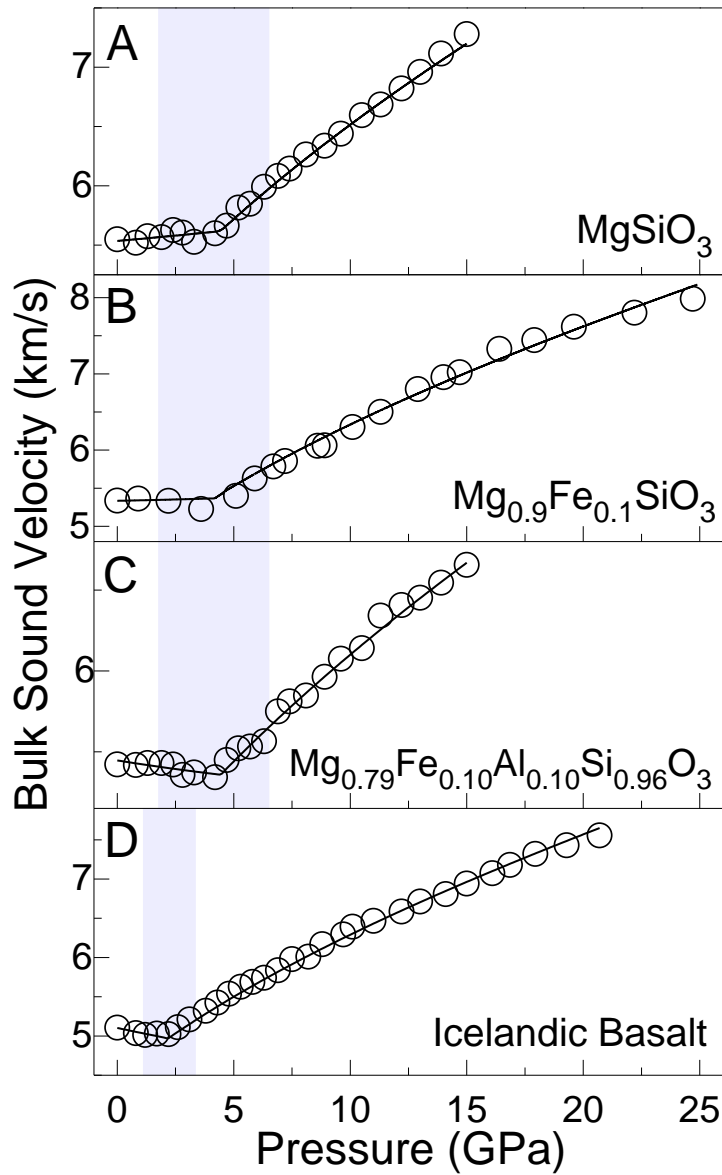
Low-Pressure State				High-Pressure State			
K_0 (GPa)	K'	G_0 (GPa)	G'	K_0 (GPa)	K'	G_0 (GPa)	G'
<i>MgSiO₃ Glass</i>							
84.2 (±1.3)	1.5 (±0.2)	43.5 (±1.5)	0.1 (±0.1)	61.2 (±2.4)	6.8 (±0.7)	32.9 (±1.7)	2.0 (±0.4)
<i>Mg_{0.9}Fe_{0.1}SiO₃ Glass</i>							
81.0 (±0.8)	1.3 (±0.2)	41.0 (±0.7)	0.3 (±0.1)	57.6 (±1.8)	6.9 (±0.6)	33.1 (±1.1)	2.0 (±0.3)
<i>Mg_{0.79}Fe_{0.10}Al_{0.10}Si_{0.96}O₃ Glass</i>							
83.3 (±1.5)	0.4 (±0.1)	40.7 (±1.2)	0.1 (±0.1)	60.0 (±2.1)	5.7 (±0.5)	32.6 (±1.3)	1.7 (±0.2)
<i>Icelandic Basalt Glass</i>							
72.8 (±0.6)	-0.6 (±0.2)	38.9 (±0.9)	-0.4 (±0.1)	56.4 (±1.4)	6.5 (±0.4)	35.8 (±0.9)	1.8 (±0.3)

77



78

79 **Figure S1.** Brillouin spectra of the silicate glasses at ambient conditions. (a) MgSiO_3 glass; (b)
 80 $\text{Mg}_{0.9}\text{Fe}_{0.1}\text{SiO}_3$ glass; (c) $\text{Mg}_{0.79}\text{Fe}_{0.10}\text{Al}_{0.10}\text{Si}_{0.96}\text{O}_3$ glass; (d) Icelandic basalt glass with a chemical
 81 composition of $\text{Na}_{0.06}\text{Ca}_{0.26}\text{Mg}_{0.26}\text{Fe}_{0.16}\text{Al}_{0.33}\text{Si}_{0.88}\text{O}_3$. Open symbols: experimental data; red solid
 82 lines: fitted results.



83

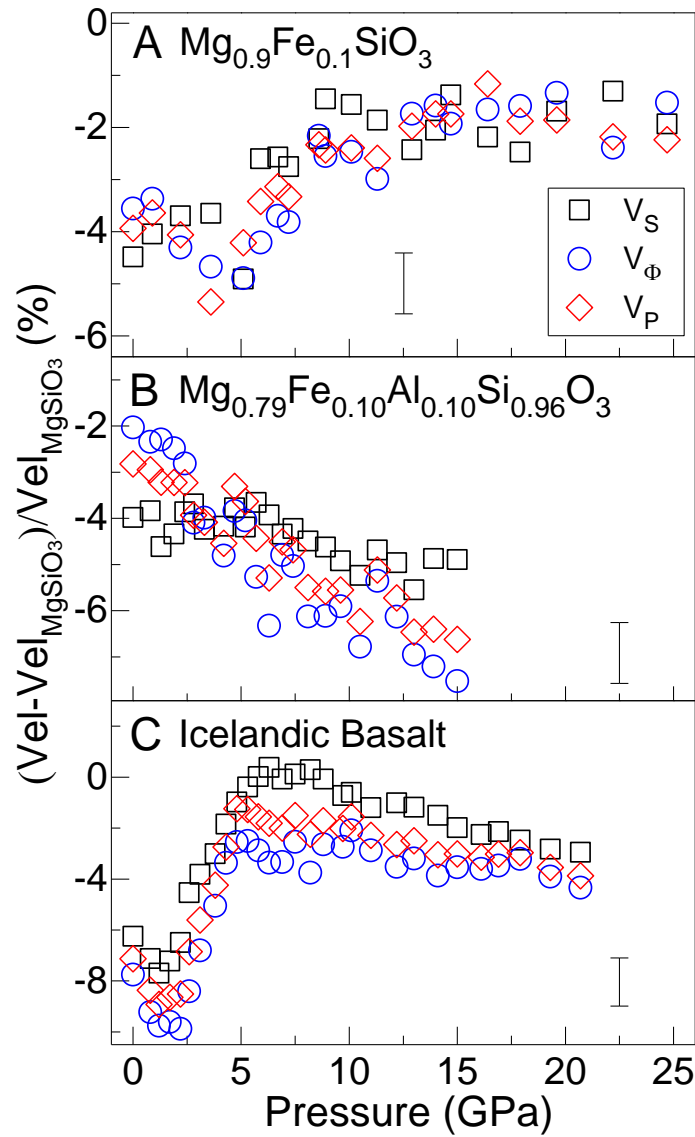
84 **Figure S2.** Bulk sound velocities (V_{ϕ}) of the glasses as a function of pressure. (a) MgSiO_3 glass;

85 (b) $\text{Mg}_{0.9}\text{Fe}_{0.1}\text{SiO}_3$ glass; (c) $\text{Mg}_{0.79}\text{Fe}_{0.10}\text{Al}_{0.10}\text{Si}_{0.96}\text{O}_3$ glass; (d) Icelandic basalt glass. Open

86 symbols: experimental bulk sound velocities obtained directly from measured V_P and V_S . Errors

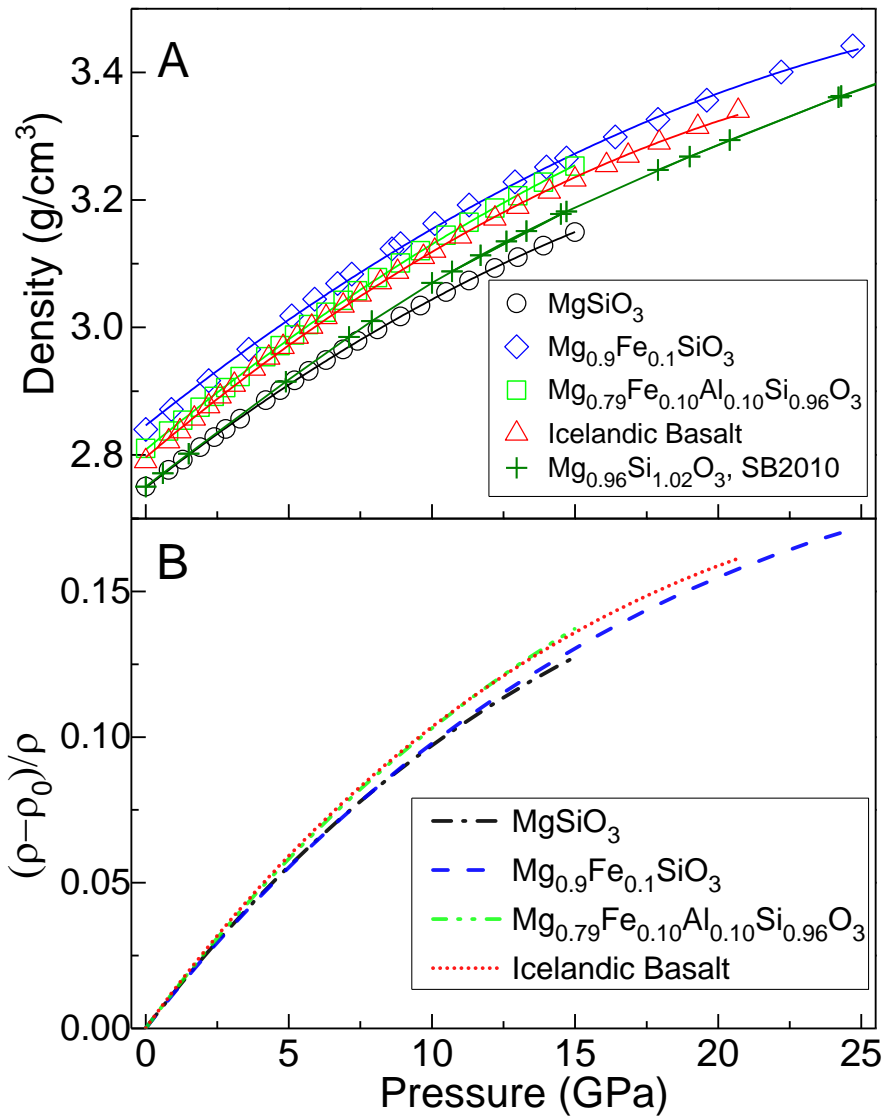
87 are smaller than the symbols and are not shown in the plots for clarity. The shaded zone represents

88 the approximate pressure range of the abnormal velocity behavior.



89

90 **Figure S3.** Velocity differences using $MgSiO_3$ glass as the standard at high pressure. (a)
 91 $Mg_{0.9}Fe_{0.1}SiO_3$ glass; (b) $Mg_{0.79}Fe_{0.10}Al_{0.10}Si_{0.96}O_3$ glass; (c) Icelandic basalt glass. Diamonds:
 92 compressional wave velocity (V_P); squares: shear wave velocity (V_S); circles: bulk sound velocity
 93 (V_ϕ); vertical ticks: representative errors ($\pm 1\sigma$) calculated using standard error propagations.



94

95 **Figure S4.** Density and relative change in density of the glasses at high pressure. (a) Density; (b)
 96 The relative change in the density ($(\rho-\rho_0)/\rho$). Circles and dash-dotted line: MgSiO₃ glass; diamonds
 97 and dashed line: Mg_{0.9}Fe_{0.1}SiO₃ glass; squares and dash-dot-dotted line: Mg_{0.79}Fe_{0.10}Al_{0.10}Si_{0.96}O₃
 98 glass; triangles and dotted: Icelandic basalt glass; pluses (+): Mg_{0.9}Fe_{0.1}SiO₃ glass, *Sanchez-Valle*
 99 *and Bass* [2010]; solid lines: modeled results.